



Statin-treated RBC dynamics in a microfluidic porous-like network

Antonios Stathouloupoulos^a, Carola S. König^b, Sudarshan Ramachandran^{b,d,e,f}, Stavroula Balabani^{a,c,*}

^a FluME, Department of Mechanical Engineering, University College London, London, UK

^b Department of Mechanical and Aerospace Engineering, Brunel University of London, Uxbridge, UK

^c UCL Hawkes Institute, University College London, London, UK

^d Department of Clinical Biochemistry, University Hospitals Birmingham NHS Foundation Trust, Birmingham, UK

^e Department of Clinical Biochemistry, University Hospitals of North Midlands, Staffordshire, UK

^f Institute for Science and Technology in Medicine, Keele University/Faculty of Health Sciences, Staffordshire University, Staffordshire, UK

ARTICLE INFO

Keywords:

RBC microscale flows
Microfluidics
microParticle tracking velocimetry
Deformability
Therapeutics
Statins

ABSTRACT

The impact of therapeutic interventions on red blood cell (RBC) deformability and microscale transport is investigated, using statins as an exemplar. Human RBCs were treated *in vitro* with two commonly prescribed statins, atorvastatin and rosuvastatin, at clinically relevant concentrations. Changes in RBC deformability were quantified using a microfluidic-based ektacytometer and expressed in terms of the elongation index. Dilute suspensions of the statin-treated RBCs were then perfused through a microfluidic pillar array, at a constant flow rate and negligible inertia, and imaged. Particle Tracking Velocimetry (PTV) was applied to track RBCs, identify preferential paths and estimate their velocities, whereas image processing was used to estimate cell dynamics, perfusion metrics and distributions. The findings were compared against those of healthy, untreated cells. Statins enhanced RBC deformability in agreement with literature. The extent of enhancement was found to be statin-dependent. The softer statin-treated cells were found to flow in straight, less tortuous paths, spend more time inside the pillar array and exhibit lower velocities compared to healthy RBCs, attributed to their enhanced deformation and longer shape recovery time upon impact with the array posts. The *in vitro* microfluidic approach demonstrated here may serve as a monitoring tool to personalise and maximise the outcome of a therapeutic treatment.

1. Introduction

Red blood cells play a key role in oxygen transport and tissue perfusion. Their function is facilitated by their unique biomechanical properties. One of these properties is RBC deformability, the ability of RBCs to alter their shape and dynamics in response to their flow environment. RBC deformability allows them to squeeze through very small capillaries; it also facilitates the margination of leukocytes and gives rise to numerous biophysical phenomena in the microcirculation (Secomb, 2017). RBC deformability is determined by the cell membrane and internal viscosity and is known to be impaired in many pathologies such as sickle cell disease, malaria, diabetes and sepsis, as well as transfusion blood storage (Barshtein et al., 2021; Baskurt et al., 1998; Connes et al., 2016; Cranston et al., 1984; Shin et al., 2007b) adversely affecting microvascular perfusion (Alexy et al., 2022). Evidence suggests that therapeutic interventions might also induce changes in the properties of

RBCs that merit further investigation. For example, cancer therapy has been found to enhance the deformation of RBCs (Cohen, 1979; Kim and Lee, 2022).

Statins are one of the most prescribed drugs in the fight against cardiovascular disease, the leading cause of mortality and morbidity worldwide. They are front-line agents to treat hypercholesterolemia (Martinez-Hervas and Ascaso, 2019), a lipid disorder in which cholesterol (low-density lipoproteins, LDL) levels are elevated in the serum, potentially leading to atherosclerosis and increased risk of cardiovascular disease (Suckling, 2014). Approximately 50 % of circulating cholesterol is carried in RBC membranes (Turner et al., 2012), playing a crucial role in their structural integrity, and regulating the membrane fluidity and stiffness (Maxfield and Tabas, 2005). When cholesterol levels are elevated, the RBC membrane lipid content also increases (Vayá et al., 2008) impacting its fluidity and function; also increasing cell internal viscosity, and leading to microvascular complications

* Corresponding author at: Department of Mechanical Engineering, University College London, London, UK.

E-mail address: s.balabani@ucl.ac.uk (S. Balabani).

<https://doi.org/10.1016/j.mvr.2024.104765>

Received 19 September 2024; Received in revised form 11 November 2024; Accepted 17 November 2024

Available online 19 November 2024

0026-2862/© 2024 The Authors. Published by Elsevier Inc. This is an open access article under the CC BY license (<http://creativecommons.org/licenses/by/4.0/>).

(Forsyth et al., 2012; Stapleton et al., 2010). Statins lead to an up-regulation of the low-density lipoprotein receptor, thus reducing serum cholesterol levels (Kolovou et al., 2008; Schwartz, 2001; Sever et al., 2003). They have also been found to reduce splenic atrophy, and bacterial infection in the spleen (Jin et al., 2013), and prevent sepsis-induced spleen apoptosis (Nezić et al., 2019). By administering statins, mortality rates of patients with chronic kidney disease (Kim et al., 2022) were found to decrease and kidney function in patients with cardiovascular diseases was improved (Esmeijer et al., 2019; Vogt et al., 2019). Statins have been reported to have antithrombotic effects and can be administered to treat blood coagulation (Undas et al., 2005).

A number of studies have associated the use of statin drugs with the softening of the RBC membrane (Forsyth et al., 2012; Sheikh-Hasani et al., 2018; Tziakas et al., 2009). However, there appears to be a lack of systematic *in vitro* studies examining the biomechanical properties of statin-treated RBCs under different flow conditions and the effect of altered cell mechanics on microscale blood flows, which are relevant to renal and splenic functions as well as tissue perfusion. There have been a number of *in vitro* studies in the literature examining the impact of RBC deformability in microhemodynamics, both numerically and experimentally. The majority of these works, including those by our group (Passos et al., 2019; Stathouloupoulos et al., 2022, 2024), have focused on the impact of impaired RBC deformability. Harder RBCs alter the rheological properties of blood (Alexy et al., 2022; Chien, 1987) and have been shown to influence transport and haematocrit distributions in microfluidic networks (Czaja et al., 2020; Ebrahimi and Bagchi, 2022). Softer RBCs have received far less attention despite evidence that softer particles alter the nature of interparticle interactions and partitioning characteristics (Shen et al., 2023).

In view of the above, the present work aims to investigate the effect of enhanced RBC deformation, induced by statin drugs, on the microscale flows of dilute RBC suspensions (5 % haematocrit level (Hct)). A simplified microfluidic geometry resembling the passage of RBCs through complex porous-like structures, such as the intervillous space of the human placenta (Chernyavsky et al., 2010; Zhou et al., 2022) (for details see the methods section) was utilised. Similar designs have been used to mimic the alveolar capillary networks (Huang et al., 2021; Stauber et al., 2017), interendothelial slits of the spleen (Dao et al., 2021; Elizalde-Torrent et al., 2021; Rigat-Brugarolas et al., 2014) and the nephron of the kidney (Sol et al., 2020; Valverde et al., 2022). Flows of healthy and statin-treated cells were imaged and velocity and cell distributions were determined to analyse the influence of enhanced RBC deformability on cell transport.

2. Experimental methods and protocols

2.1. Blood sample preparation

Blood samples were obtained from consenting human donors via venepuncture, following an approved protocol (South East London NHS Research Ethics Committee, 10/H0804/21), and mixed with 1.8 mg/mL ethylenediaminetetraacetic acid (EDTA) to prevent coagulation using appropriate vacutainers (Beckton Dickinson, UK).

RBCs were separated from whole blood through centrifugation at 3400 rpm for 9 min to remove the plasma and the buffy coat through aspiration. Then, RBCs were washed twice in phosphate buffered saline (PBS pH 7.2, Gibco, UK) using the same centrifugation protocol and resuspended at the desired Hct level using appropriate levels of PBS solution.

All samples were used within 4 h of their collection. Samples were adjusted to room temperature prior to perfusion; healthy samples were measured first, followed by statin-treated ones. Measurements reported herein were taken with samples from the same donor to avoid inter-donor variation in RBC properties.

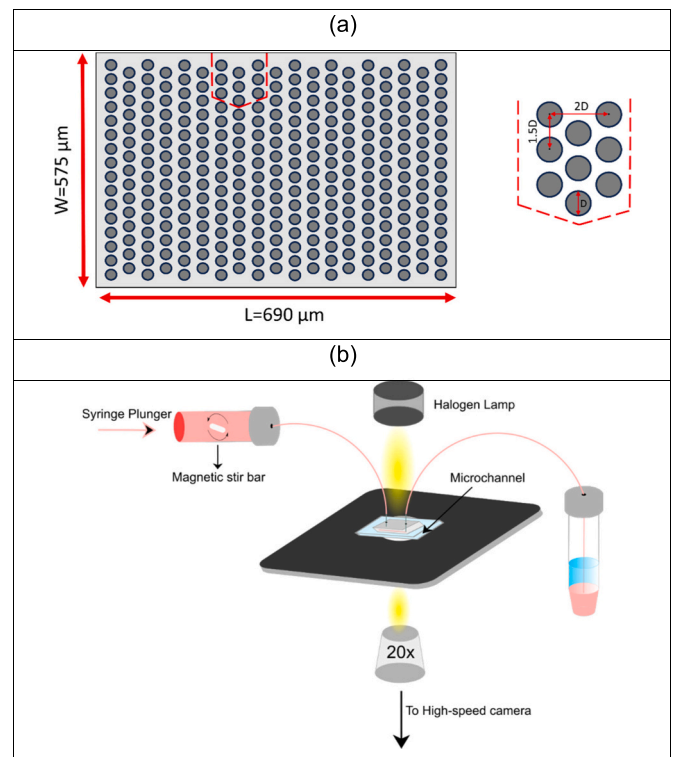


Fig. 1. (a) Top view of the microfluidic channel featuring a staggered array of cylindrical posts across the examined flow domain; RBC suspensions were perfused from the left side of the image (575 μm in width (W), 6.5 μm in height (h)) with the dashed red lines denoting a smaller region near the channel wall providing geometrical details. The diameter of each pillar (D) is 20 μm . (b) Schematic representation of the experimental setup. The pink arrow indicates the flow direction from the syringe pump. The sample was stirred gently before each measurement, and before dispensing the RBC suspensions in the microfluidic geometry, using a magnetic stir bar.

2.2. Preparation of statin solutions

Two different statins, a lipophilic (Atorvastatin, Merck, UK) and a hydrophilic (Rosuvastatin, Merck, UK) one, were utilised to prepare statin solutions and examine whether statin solubility has an effect on the transport of RBCs in microscale flow geometries. Atorvastatin and rosuvastatin were deemed suitable for the comparisons as they are the 2 most efficacious statins regarding reducing LDL cholesterol levels (Ángelo et al., 2018; Barter et al., 2010; Björkhem-Bergman et al., 2011; Cobble and Ross, 2013).

Two different protocols were followed to prepare the statin solutions, depending on the solubility of the drugs similar to (Ludolph et al., 2007; Sheikh-Hasani et al., 2018). For the lipophilic atorvastatin, the statin solution was sonicated at 37 $^{\circ}\text{C}$ for 60 min while sonication was unnecessary for solutions containing hydrophilic statins. Subsequently, RBCs were suspended in the respective statin solutions and incubated. Atorvastatin-treated RBCs (a-RBCs) were incubated in the solution for 10 min at room temperature whereas the rosuvastatin-treated RBCs (r-RBCs) were incubated at 37 $^{\circ}\text{C}$ for 30 min. Finally, the statin-treated RBCs were washed twice through centrifugation with PBS to remove any excess statins and then resuspended in PBS at a 5 % Hct level. Unlike our previous studies (Sherwood et al., 2014; Stathouloupoulos et al., 2022, 2024) in which dense suspensions were utilised to probe cell interactions, here the Ht level was lowered to enable particle tracking analysis to resolve RBC trajectories and interactions with microfluidic features.

A statin concentration of 0.7 $\mu\text{g}/\text{mL}$ was utilised, similar to previous *in vitro* studies (Ludolph et al., 2007; Sheikh-Hasani et al., 2018). This

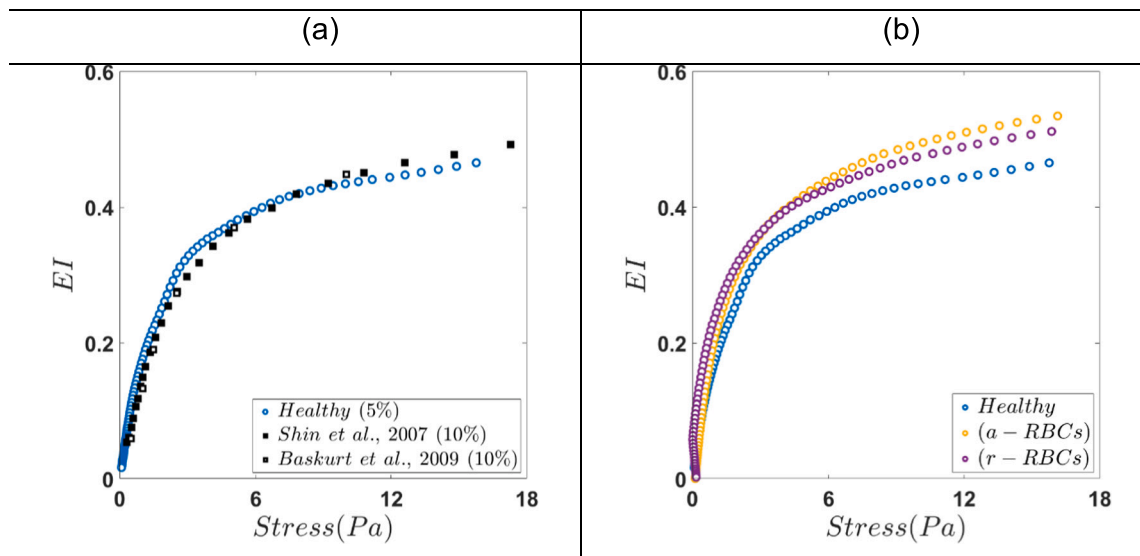


Fig. 2. *EI* curves plotted over a range of shear stresses. (a) Comparison of *EI* values for healthy RBCs in the current study against the ones reported in the literature (Baskurt et al., 2009a; Shin et al., 2007a). The Hct level of the RBC suspensions used in the deformability tests is illustrated in brackets. (b) Comparison of *EI* values between healthy (blue), atorvastatin-treated (yellow) and rosuvastatin-treated (purple) RBCs.

concentration is comparable with clinically relevant values; note that the mean concentration of statins in human serum (at therapeutic doses) is reported to be around 1–15 nmol/L (Björkhem-Bergman et al., 2011; Chou et al., 2013). The deformability of statin-treated RBCs was quantified to ascertain whether statin treatment alters RBC properties using ektacytometry as described in Section 2.5.

2.3. Microchannel fabrication

A staggered micropin configuration comprising 19 rows of 16 cylindrical posts each (20 μm in diameter D), was employed. The pitch ratios (ratio of centre-to-centre distance to pin diameter) were 2 and 1.5 in the longitudinal and transverse directions, respectively (Fig. 1(a)).

Standard soft lithography techniques were used for microchannel fabrication. Briefly, an SU-8 master was used to create microchannels from polydimethylsiloxane (PDMS, Sylgard 184, Dow, UK) prepolymer mixed with a curing agent at a 10:1 ratio. After degassing the polymer for bubble removal in a vacuum chamber, it was poured over the silicon mould (FlowJEM, US) and baked at 60 $^{\circ}\text{C}$ overnight. Subsequently, the PDMS block was peeled off and inlet and outlet holes were punched using a biopsy kit (Technical Innovations, USA). Finally, PDMS chips were bonded onto microscope glass slides using a handheld corona device (BD-20ACV, Rotaloc Inc., USA).

2.4. Image acquisition setup

Fig. 1(b) illustrates the experimental setup that was utilised to enable high-speed, brightfield imaging of the RBC flows. An inverted microscope (Nikon Diaphot 200, Japan) coupled with a high-speed camera (NanoSense MkIII, IDT, USA) and a 20 \times objective (NA = 0.4) were employed to conduct time-resolved measurements. The microchannel flow was illuminated using a 100 W halogen lamp and 1000 images were acquired for 20s at 50 Hz. RBC suspensions were perfused in the microchannels using a pneumatic syringe pump (Nemesys S, Cetoni, Germany) that has been successfully demonstrated in published microfluidic blood flow experiments (Kang et al., 2016; Zhou et al., 2020, 2022). The pneumatic syringe pump allows us to impose a flow rate rather than pressure while dispensing the fluid through the microfluidic geometry which eliminates the need to derive the flow rate from the measured velocities as in our previous studies (Stathoulopoulos et al., 2022, 2024). Image acquisition, processing and velocity estimation were

controlled using a commercially available software (DynamicStudio, Dantec Dynamics, Denmark).

The following protocol was followed to perfuse RBC suspensions in microchannels in order to reduce RBC sedimentation inside the tubing and acquire consistent data sets. Firstly, the samples were perfused at a high flow rate before each measurement to redistribute RBCs in the imaging region and then the desired flow rate was selected from the software of the flow controller. After 20 s of setting the target flow rate, image acquisition was triggered for a period of 20 s, as described in Passos et al. (2019) and van Batenburg-Sherwood and Balabani (2022) so sedimentation effects are negligible in the acquired images.

The flow rate at the channel inlet (Q_{in}) was kept constant at 0.5 $\mu\text{L}/\text{min}$ yielding a bulk flow velocity U_o of 2.2 mm/s, before entering the microfluidic network; these are within the physiological range of values for microvascular flows (Chaigneau et al., 2019; Klein et al., 2019).

2.5. RBC deformability measurements

To determine changes in RBC deformability due to statin treatment, a microfluidic-based ektacytometer (Rheoscan-D300, Sewon Meditech, Inc., Seoul, Korea) was utilized. The instrument calculates the elongation index (*EI*) of the measured cells over a range of applied shear stresses using laser-diffraction techniques. Briefly, RBCs were loaded into a disposable microfluidic cartridge and deformed as they passed through a gradually stenotic track (40 mm long, 4 mm wide and 200 μm high). Their diffraction pattern was recorded, and the *EI* was calculated. The latter is given by the ratio $(A_{\text{ellipse}} - B_{\text{ellipse}})/(A_{\text{ellipse}} + B_{\text{ellipse}})$, where A_{ellipse} and B_{ellipse} represent the major and minor axes of the deformed cell, respectively (Baskurt et al., 2009b; Shin et al., 2007a). Each suspension was measured three times using three different cartridges to ensure repeatability and to increase the significance of the acquired data.

2.6. Particle tracking velocimetry (PTV)

RBC tracking velocimetry experiments were conducted to gain insight into the motion of RBCs in the micropillar array. To extract RBC trajectories, the TrackMate tracking algorithm was utilised (Ershov et al., 2022) and the behaviour of healthy and statin-treated cells was examined. In each experiment, >1000 individual RBC tracks were

Table 1

Mean El_{max} values for healthy and statin-treated RBCs and the percentage difference between them. Differences in the reported El_{max} values between healthy and statin-treated RBCs are statistically significant ($p < 0.05$).

	Healthy RBCs	a-RBCs	r-RBCs
\bar{El}_{max} (mean \pm S.D. ^a)	0.52 \pm 0.014	0.58 \pm 0.009	0.56 \pm 0.009
Difference (%)	–	12.86	8.69

^a S.D. standard deviation.

identified. Only RBC tracks that crossed the whole micropillar domain were isolated and further processed in order to facilitate comparisons; approximately 500 tracks for each RBC suspension were thus analysed.

Table 2

Summary of studies examining changes in RBC deformability during statin treatment.

	Statin drug and concentration	Ht	RBC incubation conditions in statin solution	Deformability measurement setup	Deformability change (%)
(Sheikh-Hasani et al., 2018)	Atorvastatin 0.7 μ g/mL	Dilute human RBC suspension	10 min at room temperature	AFM	25 %
(Sheikhhasani et al., 2022)	Atorvastatin 0.1, 1 and 10 μ M	2 % human RBC suspension	10 min at 4 $^{\circ}$ C	AFM	25 %
(Ludolph et al., 2007)	Rosuvastatin 20 ng/mL	35 % human RBC suspension	30 min at 37 $^{\circ}$ C	Modified filtration method	25 %
(Forsyth et al., 2012)	Simvastatin 0.76 mg/L	1 % human RBC suspension	10 min at room temperature	Custom-made imaging setup	4 %
(Kohno et al., 1997)	Patients under pravastatin treatment	Human whole blood	–	Custom-made imaging setup	15 %

2.7. Statistical analysis

To confirm the significance of the observed trends, statistical analysis was implemented, using the Student's t -test hypothesis test. The Student's t -test is used to compare the statistical significance between the distributions of the 2 groups of data. 5 % was selected as the threshold of the p -value.

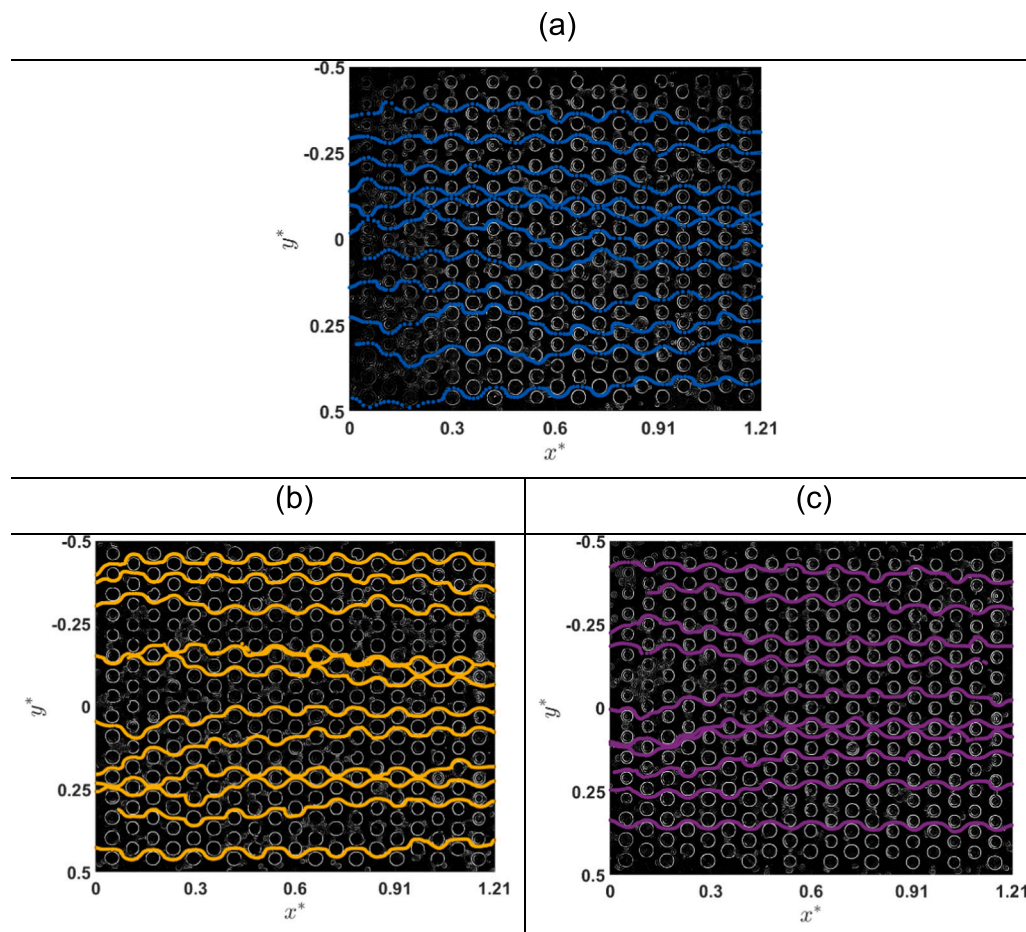


Fig. 3. Typical examples of characteristic RBC tracks in the micropillar array for (a) healthy, (b) atorvastatin-treated and (c) rosuvastatin-treated RBCs. Flow is from the left to right. The coordinates are normalised by the width of the channel $W = 575\mu\text{m}$, $x^* = x/W$, $y^* = y/W$. The coordinate system is defined such that the origin (0,0) is in the centre of the entrance of the micropillar geometry (i.e., left side of the image).

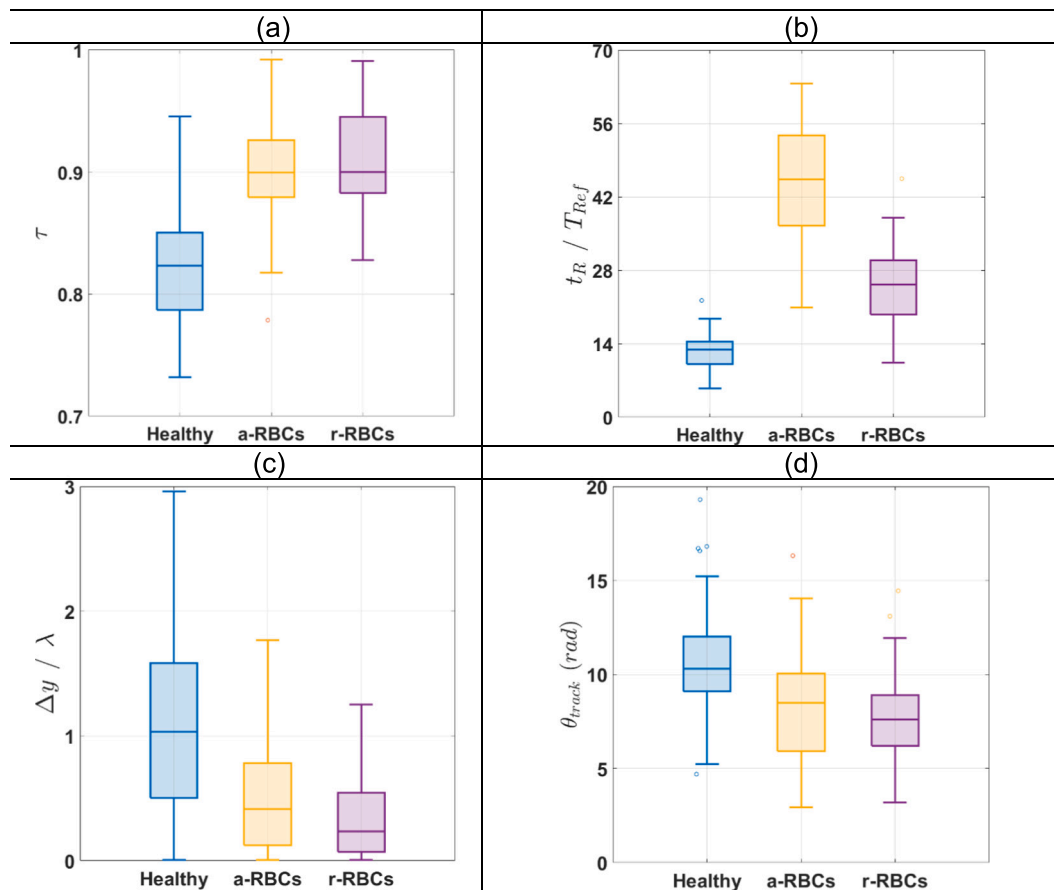


Fig. 4. Box chart summarizing (a) tortuosity (τ), (b) normalised retention time (t_R/T_{ref}) values, (c) $\Delta y/\lambda$ and (d) directional change of RBC trajectories (θ_{track}) for healthy and statin-treated RBCs. The lines inside the boxes indicate the median of the measurements and the bottom and top sides of the boxes indicate the 25th and 75th percentiles, respectively. In all cases, the differences between healthy and statin-treated RBCs are statistically significant ($p < 0.05$).

3. Results and discussion

3.1. Deformability of statin-treated RBCs

The measured elongation indices for healthy RBCs were first compared against literature for validation. Fig. 2(a) shows that EI values of healthy RBCs are in good agreement with reported values (Baskurt et al., 2009a; Shin et al., 2007a), providing confidence in the measurements and illustrating that the Hct level of the suspensions does not affect deformability measurements.

EI values for the RBCs treated with both statins are shown in Fig. 2(b) as a function of the applied stress and compared with those for healthy cells. The standard deviation of these measurements was omitted for clarity but is listed in Table 1. It is evident that RBC deformability increases for both statin treatments with the a-RBCs being the most deformable ones. The effect of statin treatment on RBC deformability becomes more pronounced when applied stresses exceed 4 Pa. At low stress values, RBCs exhibit similar EI values.

The maximum elongation index at infinite shear stress, EI_{max} was also estimated for each suspension. The mean value of three measurements and the percentage difference of the statin-treated RBCs from the healthy control group are summarised in Table 1. EI_{max} values further support that statin treatment softens the membrane of the RBCs with a-RBCs exhibiting the greatest enhancement in deformability. The measured differences are in close agreement with those reported in the literature for atorvastatin (Sheikh-Hasani et al., 2018) and rosuvastatin (Ludolph et al., 2007) treatments, respectively, as well as for simvastatin-treated RBCs (Forsyth et al., 2012). Table 2 summarises reported measurements of deformability of statin-treated RBCs. An

increase in deformability is apparent in all studies as a result of statins. Reported changes vary from 4 to 25 %. This could be partly attributed to the different techniques utilised for the measurement of deformability; ektacytometry was employed in the current study whereas optical tweezers and a modified filtration method were used by Sheikh-Hasani et al. (2018) and Ludolph et al. (2007), respectively.

3.2. RBC preferential pathways

Fig. 3 shows selected tracks of RBCs passing through the micropillar array. It is evident that healthy RBCs (Fig. 3(a)) exhibit non-straight tracks as they flow inside the examined domain. Specifically, for $y^* < 0$ healthy RBCs migrate from one axial route to the other (i.e., lane swapping event) and this trend becomes more pronounced as the cells approach the exit of the domain. In contrast, statin-treated RBCs (Fig. 3 (b), (c)) feature almost straight tracks, aligning with the flow direction, with individual cells exhibiting a decreased tendency to translocate from one row to another.

A low degree of lateral displacement of healthy RBCs flowing through porous media has also been shown by Stauber et al. (2017) in a microfluidic network similar to the one studied here, as well as in microfluidic experiments using droplets to mimic RBC flows in complex geometries (Zhou et al., 2022). Numerical simulations of Krüger et al. (2014) showed that the displacement of particles with different levels of membrane deformation leads to different preferential pathways in porous-mimicking geometries with a staggered array of pillars. They showed that softer particles follow a deterministic route inside the geometry exhibiting little displacement from one row to another, whereas more rigid particles follow a characteristic zigzag motion, leading cells

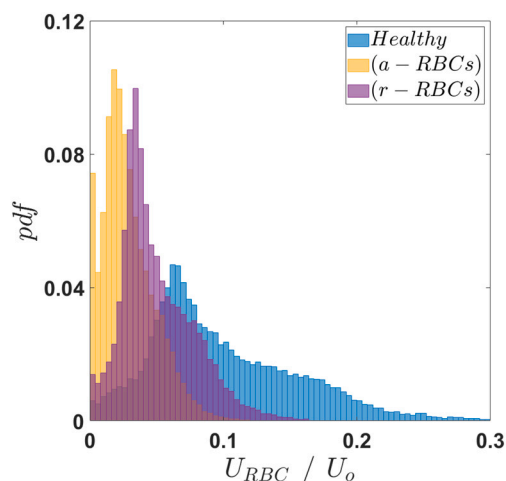


Fig. 5. Probability density function (*pdf*) of RBC suspensions with 5 % Hct flowing past through the microfluidic pillar array plotted as a function of U_{RBC}/U_o . U_{RBC} takes into account all the detected velocity magnitudes from all tracks for each RBC suspension.

to laterally shift columns along the flow direction.

An indicator of cell permeability in complex porous mimicking networks is tortuosity (τ). In this study, tortuosity is defined as the theoretical RBC displacement, assuming that RBCs move along a straight line between the entrance and the exit of the array, over the actual displacement of the cell. Values close to 1 indicate that the cell travels along a line whereas values close to 0 indicate that an RBC would traverse the flow domain. Tortuosity values are presented for healthy and statin-treated RBCs in Fig. 4(a). The latter exhibit statistically significant ($p < 0.05$) higher values (τ around 0.9) compared to the healthy RBCs, further supporting the findings in (Fig. 3(b), (c)) and indicating less tortuous paths due to statin-induced RBC softening.

The transit time of an RBC through the domain, denoted as retention time (t_R), is normalised with the reference transit time (T_{ref}) that cells require to advect the examined domain and plotted in Fig. 4(b). In each identified trajectory, a single RBC passes through the geometry and is captured by a series of successive images; t_R was calculated by dividing

the number of images by the acquisition frequency of the camera. T_{ref} is defined as $T_{ref} = L/U_o$ where $L = 1.21W$ is the length of the domain that cells traverse and U_o the inflow velocity, $U_o = Q_{in}/(Wh)$ where Q_{in} is the inlet flow rate (0.5 $\mu\text{L}/\text{min}$).

From the estimated RBC tracks, it is evident that statin-treated RBCs spend, on average, significantly more time (using the t -test analysis, $p < 0.05$) inside the micropillar array compared to the healthy ones. The importance of RBC deformability in RBC motion in complex domains is further depicted by the fact that a-RBCs spend significantly more time in the array, compared to the r-RBCs ($p < 0.05$ when comparing (t_R/T_{ref}) values between statin-treated cells in Fig. 4(b)). This underlines that although statin-treated cells exhibit on average similar tracks in terms of tortuosity (Fig. 4(a)), the increase in RBC deformability for a-RBCs leads to a statistically significant increase in RBC transit time, highlighting the correlation between RBC deformability and transit time in micropillar networks. This further implies that the changes in RBC deformability might also affect velocity distributions, which will be examined further below.

To quantify the extent of lane-swapping events of the identified RBC trajectories, the lateral displacement of each trajectory (Δy) was calculated; Δy is defined as the absolute difference, in the transverse (y^*) direction, between the entrance and the exit point of each track. Δy was then normalised against the transverse spacing (centre to centre) of the pillars, $\lambda = 1.5D$. From Fig. 4(c), it is evident that the majority of healthy RBC trajectories are displaced by at least one column in the transverse direction of the flow field whereas statin-treated cells exhibit relatively little transverse displacement. Also, the differences between a-RBCs and r-RBCs are statistically insignificant ($p > 0.05$), further supporting the tortuosity findings in Fig. 4(a).

Another metric that can characterise the impact of RBC deformability on their transport through the array is their tendency to change direction as they encounter the pillars. This can be expressed through the RBC directional change angle θ_{track} , defined as the mean value of the change in direction of each single RBC between successive images in each track. Fig. 4(d) shows that healthy RBCs exhibit the highest directional change among the three RBC suspensions, indicating that the softening of RBCs affects their dynamics as they are transported through the array. In line with the findings in Fig. 4(a) and (c), no statistically significant difference was evident between a-RBCs and r-RBCs, respectively, explaining the less tortuous tracks and less lane-swapping events

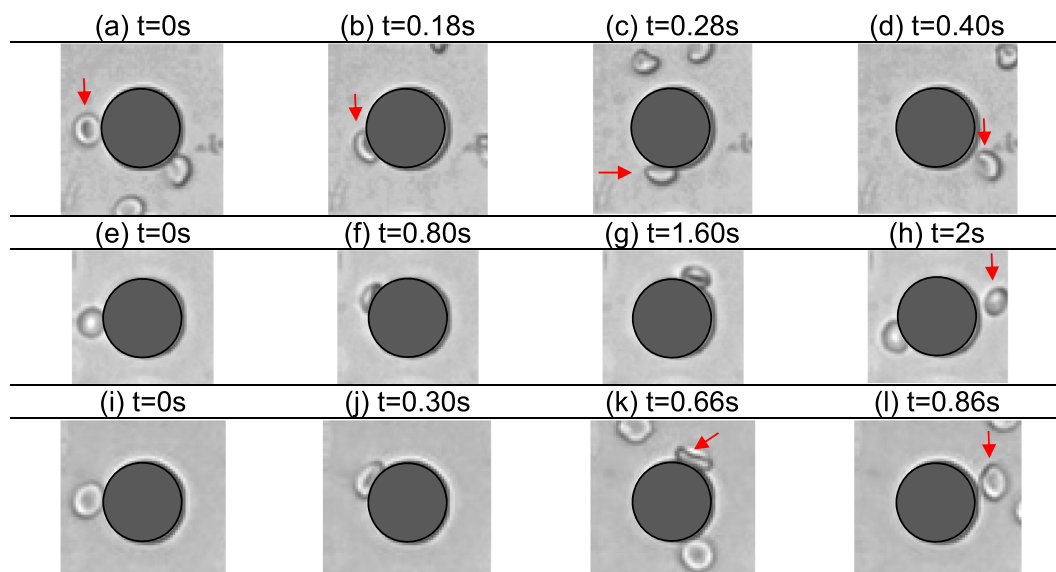


Fig. 6. Snapshots of RBCs (Hct: 5%) colliding with a single circular post of the microfluidic geometry. The location of the pillar is illustrated in Fig. 1(b) and the motion of cells is from the left to right. (a)–(d) illustrate healthy RBCs, (e)–(h) a-RBCs and (h)–(l) r-RBCs. The red arrows are used for clarity and guide the reader to detect the single RBCs. Flow enters from the left side of the figures and exits from the right side.

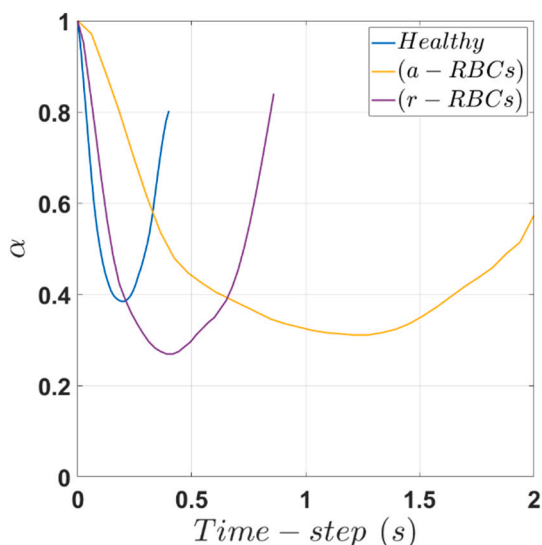


Fig. 7. RBC shape recovery index (α), for a single cell, for healthy (blue), atorvastatin-treated (yellow) and rosuvastatin-treated (purple) RBCs colliding with a single, circular post of the microfluidic geometry.

along the flow direction found.

To further characterise the transport of RBCs through the microfluidic network, their instantaneous velocities (U_{RBC}) were determined and their probability density function (*pdf*) was plotted and shown in Fig. 5. To facilitate comparisons, U_{RBC} was normalised with the velocity at the inlet of the geometry U_o . It should be noted that the applied flow rate of RBC suspensions was kept constant and equal to 0.5 $\mu\text{L}/\text{min}$ for all the examined cases.

The normalised velocity distributions of healthy RBCs (Fig. 5) show that they move faster compared to the statin-treated ones. The softer cells, i.e. a-RBCs, are the slowest of the three. Healthy cells exhibit a wider velocity distribution compared to statin-treated ones. The velocities of the statin-treated RBCs are distributed in a relatively narrow band and show a high degree of overlap, indicating that as RBC deformability increases, cells slow down, exhibiting similar low velocities throughout the domain. Interestingly, the histogram for the a-RBCs illustrates a large peak close to $U_{RBC} = 0$. This is due to the trend of slow-moving soft RBCs being trapped as they collide with the posts as can be seen in the acquired images in Fig. 6, discussed further in this section. Although many cells seem to be travelling with near-zero velocities, especially a-RBCs, these events become less frequent with a decrease in

RBC deformability illustrating that RBC transport in the pillar arrays is heterogeneous and dynamic and strongly dependent on cell deformability. The distributions in Fig. 5 further corroborate the findings in Fig. 4(b) implying that as cell deformation increases, RBC instantaneous velocity decreases and cells spend more time inside the micropillar domain. The findings are in agreement with the computational work of Krüger et al. (2014), illustrating that softer cells develop lower velocities as they pass through a porous medium compared to more rigid ones.

To gain insight into the impact of RBC collisions with the circular posts and understand the high number of near-zero velocities in Fig. 5, individual snapshots of single cells were isolated from the acquired images. Healthy RBCs (Fig. 6(a)–(d)) tend to collide and escape from the near-post region much quicker than statin-treated cells. It is also evident that healthy cells deform and change their shape into a parachute-like structure before leaving the micro-pillar array.

a-RBCs, which are the most deformable ones, can be seen to collide with the pillar, start changing shape (Fig. 6(e)–(f)) and slide along the wall in the flow direction (Fig. 6(g)). Eventually, they escape from the near-wall area but their motion after impacting the post is significantly slower compared to the healthy ones (Fig. 6(h)), reflected in the estimated transit times. Similarly, r-RBCs are seen in Fig. 6(i)–(l) to spend more time near the pillars compared to the healthy ones.

It becomes apparent that changes in RBC deformability due to statin treatment can affect the nature of heterogeneous collisions between RBCs and posts. Krüger et al. (2014) showed numerically that changes in RBC deformability impact the shape cells adopt along the flow direction past collisions with the posts. They found that the more deformable RBCs become, the more their diameter decreases affecting their trajectory. This reduces RBC transverse motion from one column to another leading to a more deterministic RBC motion inside the pillar geometry. This can also be observed in Fig. 6 -note the diameter of statin-treated cells (i.e., Fig. 6(f), (g), (j), (k)) is reduced compared to the healthy ones (i.e., Fig. 6(b), (c)) after colliding with the pillar- and further quantified by estimating the change in RBC shape (A_{RBC}).

This was done by locating individual cells in Fig. 6, binarizing them and estimating their area. The calculated values were averaged and normalised with the initial cell area ($A_{RBC,0}$), prior to colliding with the pillar, defining thus an RBC shape recovery index, $\alpha = A_{RBC}/A_{RBC,0}$ plotted in Fig. 7 for all RBCs investigated.

Healthy RBCs can be seen to collide with the circular pillars, and almost recover their initial shape in <0.5 s whereas statin-treated cells take more time to return to their original size. Interestingly, a-RBCs take the longest time to recover, and the final cell size is the least recovered out of the three examined RBC suspensions. Thus, as RBC deformability increases, individual cells take more time to return to their original shape after colliding with a rigid obstacle. Moreover, softer cells deform

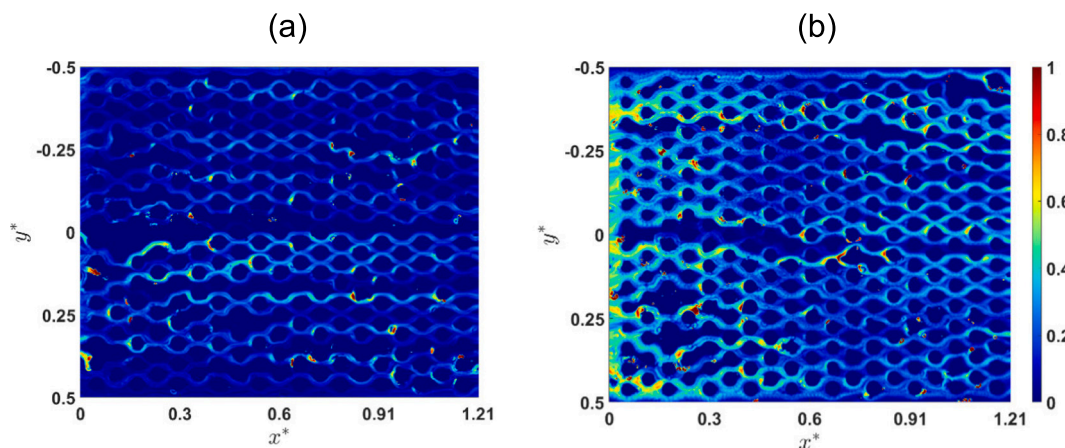


Fig. 8. Indicative maps illustrating the probability of the detected RBCs to be in the same location of (a) healthy and (b) a-RBCs in the micropillar array. Flow is from left to right.

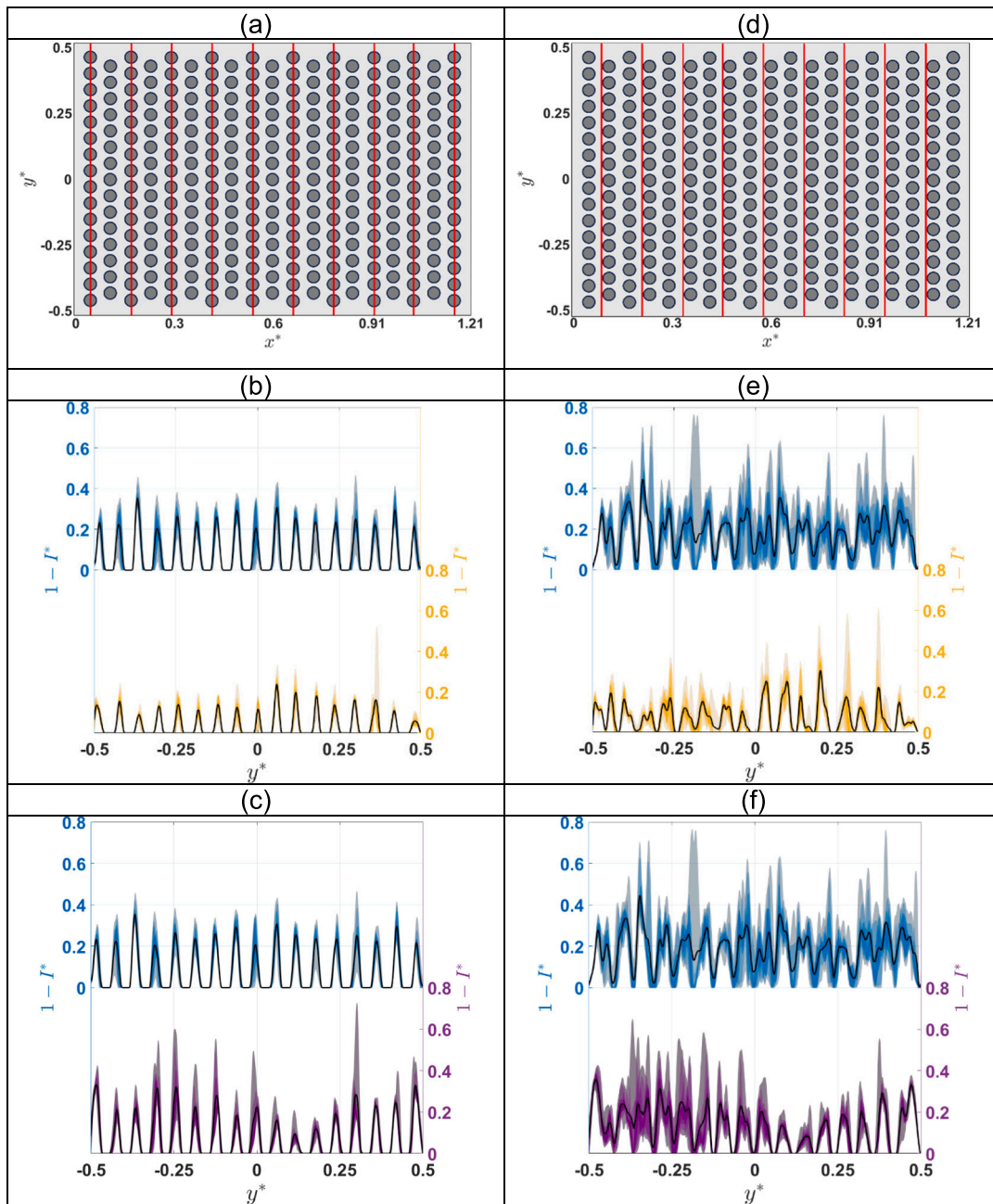


Fig. 9. (a) (d) Axial x^* -locations (red solid lines) in the pillar array selected to illustrate cell distributions, expressed via image intensity $1 - I^*$. (b), (c), (e), (f) Fan charts summarizing all measured $1 - I^*$ profiles in the selected axial positions for healthy (blue), a-RBCs (yellow) and r-RBCs (purple). Each subplot compares healthy RBC distributions against statin treated ones, i.e. (b), (e) compares healthy against a-RBCs and (c), (f) healthy against r-RBC suspensions. Black lines indicate the mean value of the measurements and the shaded bands distribution percentiles. The left panel corresponds to cell distributions between pillars in alternative rows (locations shown in Fig. 9a) whereas the right panel to cell distributions between rows, very close to the pillars (locations shown in Fig. 9b).

more upon colliding with the pillars and spend significantly more time around the pillar region by flipping and sliding along the pillar wall, which explains the lower velocities observed for the statin-treated RBCs.

3.3. Local distributions of statin-treated cells

The spatial organisation of the RBCs in the pillar arrays is illustrated in the form of colourmaps in Fig. 8, showing the probability of the detected RBCs being in the same location. To produce these colourmaps the acquired images were binarized so that RBC areas were assigned values of 1 whereas the rest of the image values of 0 and time-averaged. Thus, if an RBC, during the period of the acquisition, was detected in the

same location then the colormap value will be close to 1. If an RBC flows past a specific region in a way that is rarely detected in the same position, then the colormap value will be close to zero. The differences between healthy and a-RBCs are clearly illustrated as they transit the pillar array. The colourmaps show near zero probability for healthy RBCs to be in the same location between successive images and higher probabilities for the slower moving statin treated cells, reflecting the local RBC dynamics and transit time characteristics discussed in the previous section.

Local RBC concentrations were also inferred from the time-averaged images of each suspension and fan charts were utilised to show cumulative results. The mean intensity values were normalised by the maximum image intensity in the area outside of the channel (I_{max}), i.e.

$I^* = I_{raw}/I_{max}$, and expressed in terms of $1 - I^*$ so that darker regions correspond to higher cell concentration and zero cell concentration corresponds to the presence of a pillar.

Typical distributions for selected rows (i.e., illustrated in Fig. 9(a)) are shown in Fig. 9(b) and (c) comparing healthy RBCs against a- and r-RBC suspensions, respectively. The distribution of healthy cells between adjacent pillars in a row appears uniform, a trend that is also evident for flows of healthy cells around pillars in wider geometries (Stathouloupoulos et al., 2022), and in agreement with the trajectories of the healthy cells. On the other hand, statin treated cells exhibit less uniform distributions across the row compared to healthy cells and the effect is more pronounced for the r-statin treated cells. This can be attributed to the enhanced tendency to collide with the pillars, as well as their deformation and shape recovery post collision (Fig. 6). The impact of cell deformability is further depicted by the enhanced concentration of r-RBCs compared to a-RBCs (Fig. 9(b), (c)); this can be attributed to the reduced retention time r-RBCs experience as they pass through the array resulting in r-RBCs flowing in the interpillar spacing, unlike a-RBCs that collide with the posts. Furthermore, a-RBCs exhibit longer shape recovery times and might cross the gap between pillars while still deformed resulting in a lower $1 - I^*$ value recorded therein compared to r-RBCs.

Cell distributions between successive rows - i.e. in the pillar wakes (Fig. 9d) - exhibit higher fluctuations compared to those between pillars as shown in Fig. 9(e)–(f), which can be attributed to the fact that the flow is less confined compared to the gap flows. Despite the variation with axial location the general trends between healthy and statin treated cells are similar to those observed in between pillars.

4. Conclusions

The impact of treating RBCs with two commonly prescribed statins, atorvastatin and rosuvastatin, on their deformation and transport through a pillar array was experimentally investigated. The deformability of the treated RBCs was quantified using a microfluidic-based ektacytometer and found to be enhanced by at least 9% compared to healthy ones.

RBC transport was studied by means of Particle Tracking Velocimetry. The trajectories of statin-treated cells were found to be more deterministic compared to healthy ones. Specifically, statin-treated RBCs could traverse the array with little lateral displacement featuring straight tracks along the flow direction, unlike healthy RBCs. As a result, a higher tortuosity index was estimated for healthy cells compared to statin-treated ones. However, although both statin-treated cells exhibit similar tortuosity indices, a-RBCs spent significantly more time inside the micropillar array due to the impact of RBC deformability on RBC collisions with rigid obstacles.

Due to the nature of these collisions, statin-treated cells were found to exhibit lower cell velocities compared to healthy ones, as they passed through the geometry. The softer statin-treated RBCs deform more compared to healthy ones around the pillars and they recover their shape slower, which leads to an increase in the probability of near-zero velocities and their retention time in the array compared to the healthy ones.

Local cell distributions revealed that healthy cells are more uniformly distributed in the interstitial space between pillars and exhibit higher concentration fluctuations in between rows, compared to statin-treated ones. r-RBCs were found to exhibit higher cell concentration between pillars and more heterogeneous distribution compared to a-RBCs.

The study illustrates that statins enhance the deformability of RBCs, altering perfusion through complex microfluidic networks. While statins are prescribed to lower the risk of vascular events, this enhanced deformability might be beneficial for patients with comorbidities such as diabetes or conditions such as Alzheimer's known to impair RBC

deformability and impact microvascular flow. The study shows that changes in RBC deformability are statin-dependent which implies that potential benefits of statins might be heterogeneous.

Finally, the findings of this study might have implications for other routine treatments for example testosterone therapy (TTh), that may result in a notable change in RBC deformability. The *in vitro* approach illustrated in this study provides a platform to examine the impact of such treatments and may serve as a monitoring tool for the efficacy of such therapeutic treatments, paving the way for personalised medicine.

CRedit authorship contribution statement

Antonios Stathouloupoulos: Writing – review & editing, Writing – original draft, Software, Methodology, Investigation, Formal analysis, Data curation, Conceptualization. **Carola S. König:** Writing – review & editing, Writing – original draft, Investigation, Conceptualization. **Sudarshan Ramachandran:** Writing – review & editing, Methodology, Investigation, Conceptualization. **Stavroula Balabani:** Writing – review & editing, Writing – original draft, Supervision, Resources, Project administration, Methodology, Investigation, Funding acquisition, Formal analysis, Data curation, Conceptualization.

Declaration of competing interest

The authors declare the following financial interests/personal relationships which may be considered as potential competing interests: Stavroula Balabani reports financial support was provided by UK Research and Innovation. If there are other authors, they declare that they have no known competing financial interests or personal relationships that could have appeared to influence the work reported in this paper.

Acknowledgements

The authors would like to thank the blood donor who took part in this study. Financial support from the EPSRC DTP programme (EP/R513143/1) and the Future Blood Testing Network+ (EP/W000652/1) are gratefully acknowledged.

Data availability

Data will be made available on request.

References

- Alexy, T., Detterich, J., Connes, P., Toth, K., Nader, E., Kenyeres, P., Arriola-Montenegro, J., Ulker, P., Simmonds, M.J., 2022. Physical properties of blood and their relationship to clinical conditions. *Front. Physiol.* 13 (July), 1–15. <https://doi.org/10.3389/fphys.2022.906768>.
- Angelo, M.L., Moreira, F. de L., Morais Ruela, A.L., Santos, A.L.A., Salgado, H.R.N., de Araújo, M.B., 2018. Analytical methods for the determination of rosuvastatin in pharmaceutical formulations and biological fluids: a critical review. *Crit. Rev. Anal. Chem.* 48 (4), 317–329. <https://doi.org/10.1080/10408347.2018.1439364>.
- Barshstein, G., Pajic-Lijakovic, I., Gural, A., 2021. Deformability of stored red blood cells. *Front. Physiol.* 12 (September), 1–13. <https://doi.org/10.3389/fphys.2021.722896>.
- Barter, P.J., Brandrup-Wognsen, G., Palmer, M.K., Nicholls, S.J., 2010. Effect of statins on HDL-C: a complex process unrelated to changes in LDL-C: analysis of the VOYAGER Database. *J. Lipid Res.* 51 (6), 1546–1553. <https://doi.org/10.1194/jlr.P002816>.
- Baskurt, O.K., Gelmont, D., Meiselman, H.J., 1998. Red blood cell deformability in sepsis. *Am. J. Respir. Crit. Care Med.* 157 (2), 421–427. <https://doi.org/10.1164/ajrccm.157.2.9611103>.
- Baskurt, O.K., Hardeman, M.R., Uykulu, M., Ulker, P., Cengiz, M., Nemeth, N., Shin, S., Alexy, T., Meiselman, H.J., 2009a. Comparison of three commercially available ektacytometers with different shearing geometries. *Biorheology* 46 (3), 251–264. <https://doi.org/10.3233/BIR-2009-0536>.
- Baskurt, O.K., Hardeman, M.R., Uykulu, M., Ulker, P., Cengiz, M., Nemeth, N., Shin, S., Alexy, T., Meiselman, H.J., 2009b. Parameterization of red blood cell elongation index - shear stress curves obtained by ektacytometry. *Scand. J. Clin. Lab. Invest.* 69 (7), 777–788. <https://doi.org/10.3109/00365510903266069>.

- Björkhem-Bergman, L., Lindh, J.D., Bergman, P., 2011. What is a relevant statin concentration in cell experiments claiming pleiotropic effects? *Br. J. Clin. Pharmacol.* 72 (1), 164–165. <https://doi.org/10.1111/j.1365-2125.2011.03907.x>.
- Chaigneau, E., Roche, M., Charpak, S., 2019. Unbiased analysis method for measurement of red blood cell size and velocity with laser scanning microscopy. *Front. Neurosci.* 13 (JUN), 1–9. <https://doi.org/10.3389/fnins.2019.00644>.
- Chernyavsky, I.L., Jensen, O.E., Leach, L., 2010. A mathematical model of Intervillous blood flow in the human placenta. *Placenta* 31 (1), 44–52. <https://doi.org/10.1016/j.placenta.2009.11.003>.
- Chien, S., 1987. Red cell deformability and its relevance to blood flow. *Annu. Rev. Physiol.* 49 (1), 177–192. <https://doi.org/10.1146/annurev.ph.49.030187.001141>.
- Chou, Y.-C., Wang, Y.-K., Chang, M.-J., Ueng, Y.-F., 2013. Determination of serum atorvastatin concentrations in lipid-controlling patients with and without myalgia syndrome. *J. Food Drug Anal.* 21 (2), 147–153. <https://doi.org/10.1016/j.jfda.2013.05.003>.
- Cobble, M., Ross, J., 2013. Individualizing statin. *Therapy* 23 (2), 1–8.
- Cohen, M.H., 1979. Impairment of red blood cell deformability by tumor growth. *JNCI J. Natl. Cancer Inst.* 63 (2), 525–526. <https://doi.org/10.1093/jnci/63.2.525>.
- Connes, P., Alexy, T., Deterlich, J., Romana, M., Hardy-Dessources, M.-D., Ballas, S.K., 2016. The role of blood rheology in sickle cell disease. *Blood Rev.* 30 (2), 111–118. <https://doi.org/10.1016/j.blr.2015.08.005>.
- Cranston, H.A., Boylan, C.W., Carroll, G.L., Sutura, S.P., Williamson, J.R., Gluzman, I.Y., Krogstad, D.J., 1984. Plasmodium falciparum maturation abolishes physiologic red cell deformability. *Science* 223 (4634), 400–403. <https://doi.org/10.1126/science.6362007>.
- Czaja, B., Gutierrez, M., Závodszy, G., De Kanter, D., Hoekstra, A., Eniola-Adefeso, O., 2020. The influence of red blood cell deformability on hematocrit profiles and platelet margination. *PLoS Comput. Biol.* 16 (3), e1007716. <https://doi.org/10.1371/journal.pcbi.1007716>.
- Dao, M., MacDonald, I., Asaro, R.J., 2021. Erythrocyte flow through the interendothelial slits of the splenic venous sinus. *Biomech. Model. Mechanobiol.* 20 (6), 2227–2245. <https://doi.org/10.1007/s10237-021-01503-y>.
- Ebrahimi, S., Bagchi, P., 2022. A computational study of red blood cell deformability effect on hemodynamic alteration in capillary vessel network. *Sci. Rep.* 12 (1), 4304. <https://doi.org/10.1038/s41598-022-08357-z>.
- Elizalde-Torrent, A., Trejo-Soto, C., Méndez-Mora, L., Nicolau, M., Ezama, O., Gualdrón-López, M., Fernández-Becerra, C., Alarcón, T., Hernández-Machado, A., del Portillo, H.A., 2021. Pitting of malaria parasites in microfluidic devices mimicking spleen interendothelial slits. *Sci. Rep.* 11 (1), 22099. <https://doi.org/10.1038/s41598-021-01568-w>.
- Ershov, D., Phan, M.-S., Pylvänäinen, J.W., Rigaud, S.U., Le Blanc, L., Charles-Orszag, A., Conway, J.R.W., Laine, R.F., Roy, N.H., Bonazzi, D., Duménil, G., Jacquemet, G., Tinevez, J.-Y., 2022. TrackMate 7: integrating state-of-the-art segmentation algorithms into tracking pipelines. *Nat. Methods* 19 (7), 829–832. <https://doi.org/10.1038/s41592-022-01507-1>.
- Esmeijer, K., Dekkers, O.M., de Fijter, J.W., Dekker, F.W., Hoogeveen, E.K., 2019. Effect of different types of statins on kidney function decline and proteinuria: a network meta-analysis. *Sci. Rep.* 9 (1), 16632. <https://doi.org/10.1038/s41598-019-53064-x>.
- Forsyth, A.M., Braunmüller, S., Wan, J., Franke, T., Stone, H.A., 2012. The effects of membrane cholesterol and simvastatin on red blood cell deformability and ATP release. *Microvasc. Res.* 83 (3), 347–351. <https://doi.org/10.1016/j.mvr.2012.02.004>.
- Huang, D., Liu, T., Liao, J., Maharjan, S., Xie, X., Pérez, M., Anaya, I., Wang, S., Tirado Mayer, A., Kang, Z., Kong, W., Mainardi, V.L., Garciamendez-Mijares, C.E., García Martínez, G., Moretti, M., Zhang, W., Gu, Z., Ghaemmaghami, A.M., Zhang, Y.S., 2021. Reversed-engineered human alveolar lung-on-a-chip model. *Proc. Natl. Acad. Sci.* 118 (19), e2016146118. <https://doi.org/10.1073/pnas.2016146118>.
- Jin, R., Zhu, X., Liu, L., Nanda, A., Granger, D.N., Li, G., 2013. Simvastatin attenuates stroke-induced splenic atrophy and lung susceptibility to spontaneous bacterial infection in mice. *Stroke* 44 (4), 1135–1143. <https://doi.org/10.1161/STROKEAHA.111.000633>.
- Kang, Y.J., Ha, Y.-R., Lee, S.-J., 2016. Deformability measurement of red blood cells using a microfluidic channel array and an air cavity in a driving syringe with high throughput and precise detection of subpopulations. *Analyst* 141 (1), 319–330. <https://doi.org/10.1039/C5AN01988E>.
- Kim, Y.K., Lee, J.M., 2022. Change of RBC deformability during hematopoietic stem cell transplantation. *J. Pediatr. Hematol. Oncol.* 44 (2), e329–e333. <https://doi.org/10.1097/MPH.0000000000002295>.
- Kim, J.E., Choi, Y.J., Oh, S.W., Kim, M.G., Jo, S.K., Cho, W.Y., Ahn, S.Y., Kwon, Y.J., Ko, G.-J., 2022. The effect of statins on mortality of patients with chronic kidney disease based on data of the observational medical outcomes partnership common data model (OMOP-CDM) and Korea National Health Insurance Claims Database. *Frontiers in Nephrology* 1. <https://doi.org/10.3389/fneph.2021.821585>.
- Klein, S.P., De Sloovere, V., Meyfroidt, G., Depreitere, B., 2019. Autoregulation assessment by direct visualisation of pial arterial blood flow in the piglet brain. *Sci. Rep.* 9 (1), 13333. <https://doi.org/10.1038/s41598-019-50046-x>.
- Kohno, M., Murakawa, K., Yasunari, K., Yokokawa, K., Horio, T., Kano, H., Minami, M., Yoshikawa, J., 1997. Improvement of erythrocyte deformability by cholesterol-lowering therapy with pravastatin in hypercholesterolemic patients. *Metabolism* 46 (3), 287–291. [https://doi.org/10.1016/S0026-0495\(97\)90255-9](https://doi.org/10.1016/S0026-0495(97)90255-9).
- Kolovou, G.D., Vasilidiadis, I., Anagnostopoulou, K., Cokkinos, D.V., 2008. Simvastatin: two decades in a circle. *Cardiovasc. Ther.* 26 (2), 166–178. <https://doi.org/10.1111/j.1527-3466.2008.00047.x>.
- Krüger, T., Holmes, D., Coveney, P.V., 2014. Deformability-based red blood cell separation in deterministic lateral displacement devices—a simulation study. *Biomicrofluidics* 8 (5), 054114. <https://doi.org/10.1063/1.4897913>.
- Ludolph, B., Bloch, W., Kelm, M., Schulz, R., Kleinbongard, P., 2007. Short-term effect of the HMG-CoA reductase inhibitor rosuvastatin on erythrocyte nitric oxide synthase activity. *Vasc. Health Risk Manag.* 3 (6), 1069–1073. <http://www.ncbi.nlm.nih.gov/pubmed/18200826>.
- Martinez-Hervas, S., Ascaso, J.F., 2019. Hypercholesterolemia. In: *Encyclopedia of Endocrine Diseases*. Elsevier, pp. 320–326. <https://doi.org/10.1016/B978-0-12-801238-3.65340-0>.
- Maxfield, F.R., Tabas, I., 2005. Role of cholesterol and lipid organization in disease. *Nature* 438 (7068), 612–621. <https://doi.org/10.1038/nature04399>.
- Nežić, L., Amidžić, L., Škrbić, R., Gajanić, R., Nepovimova, E., Vališ, M., Kuća, K., Jacević, V., 2019. Simvastatin inhibits endotoxin-induced apoptosis in liver and spleen through up-regulation of survivin/NF-κB/p65 expression. *Front. Pharmacol.* 10. <https://doi.org/10.3389/fphar.2019.00054>.
- Passos, A., Sherwood, J.M., Kaliviotis, E., Agrawal, R., Pavesio, C., Balabani, S., 2019. The effect of deformability on the microscale flow behavior of red blood cell suspensions. *Phys. Fluids* 31 (9), 91903. <https://doi.org/10.1063/1.5111189>.
- Rigat-Brugarolas, L.G., Elizalde-Torrent, A., Bernabeu, M., De Niz, M., Martín-Jaular, L., Fernández-Becerra, C., Homs-Corbera, A., Samitier, J., del Portillo, H.A., 2014. A functional microengineered model of the human spleen-on-a-chip. *Lab Chip* 14 (10), 1715–1724. <https://doi.org/10.1039/C3LC51449FH>.
- Schwartz, G.G., 2001. Effects of atorvastatin on early recurrent ischemic events in acute coronary syndromes. The MIRACL study: a randomized controlled trial. *JAMA* 285 (13), 1711. <https://doi.org/10.1001/jama.285.13.1711>.
- Secomb, T.W., 2017. Blood flow in the microcirculation. *Annu. Rev. Fluid Mech.* 49 (1), 443–461. <https://doi.org/10.1146/annurev-fluid-010816-060302>.
- Sever, P.S., Dahlöf, B., Poulter, N.R., Wedel, H., Beevers, G., Caulfield, M., Collins, R., Kjeldsen, S.E., Kristinsson, A., McInnes, G.T., Mehlsen, J., Nieminen, M., O'Brien, E., Östergren, J., 2003. Prevention of coronary and stroke events with atorvastatin in hypertensive patients who have average or lower-than-average cholesterol concentrations, in the Anglo-Scandinavian Cardiac Outcomes Trial—Lipid Lowering Arm (ASCOT-LLA): a multicentre randomised. *Lancet* 361 (9364), 1149–1158. [https://doi.org/10.1016/S0140-6736\(03\)12948-0](https://doi.org/10.1016/S0140-6736(03)12948-0).
- Sheikh-Hasani, V., Babaei, M., Azadbakht, A., Pazoki-Toroudi, H., Mashaghi, A., Moosavi-Movahedi, A.A., Reihani, S.N.S., 2020. Atorvastatin treatment softens human red blood cells: an optical tweezers study. *Biomed. Opt. Express* 9 (3), 1256. <https://doi.org/10.1364/BOE.9.001256>.
- Sheikhkhassani, V., Evers, T.M.J., Lamba, S., Shokri, F., Mashaghi, A., 2022. Single cell force spectroscopy of erythrocytes at physiological and febrile temperatures reveals mechano-modulatory effects of atorvastatin. *Soft Matter* 18 (11), 2143–2148. <https://doi.org/10.1039/D1SM01715B>.
- Shen, Z., Plouraboué, F., Lintuvuori, J.S., Zhang, H., Abbasi, M., Misbah, C., 2023. Anomalous diffusion of deformable particles in a honeycomb network. *Phys. Rev. Lett.* 130 (1), 014001. <https://doi.org/10.1103/PhysRevLett.130.014001>.
- Sherwood, J.M., Holmes, D., Kaliviotis, E., Balabani, S., 2014. Spatial distributions of red blood cells significantly alter local haemodynamics. *PLoS One* 9 (6), e100473. <https://doi.org/10.1371/journal.pone.0100473>.
- Shin, S., Hou, J.X., Suh, J.S., Singh, M., 2007a. Validation and application of a microfluidic ektacytometer (RheoScan-D) in measuring erythrocyte deformability. *Clin. Hemorheol. Microcirc.* 37 (4), 319–328.
- Shin, Seh-yun, Ku, Y.H., Ho, J.X., Kim, Y.K., Suh, J.S., Singh, M., 2007b. Progressive impairment of erythrocyte deformability as indicator of microangiopathy in type 2 diabetes mellitus. *Clin. Hemorheol. Microcirc.* 36 (3), 253–261. <http://www.ncbi.nlm.nih.gov/pubmed/17361027>.
- Sol, M., Kamps, J.A.A.M., van den Born, J., van den Heuvel, M.C., van der Vlag, J., Krenning, G., Hillebrands, J.-L., 2020. Glomerular endothelial cells as instigators of glomerular sclerotic diseases. *Front. Pharmacol.* 11 (October), 1–13. <https://doi.org/10.3389/fphar.2020.573557>.
- Stapleton, P.A., Goodwill, A.G., James, M.E., Brock, R.W., Frisbee, J.C., 2010. Hypercholesterolemia and microvascular dysfunction: interventional strategies. *J. Inflamm.* 7 (1), 54. <https://doi.org/10.1186/1476-9255-7-54>.
- Stathouloupoulos, A., Passos, A., Balabani, S., 2022. Flows of healthy and hardened RBC suspensions through a micropillar array. *Med. Eng. Phys.* 107, 103874. <https://doi.org/10.1016/j.medengphy.2022.103874>.
- Stathouloupoulos, A., Passos, A., Kaliviotis, E., Balabani, S., 2024. Partitioning of dense RBC suspensions in single microfluidic bifurcations: role of cell deformability and bifurcation angle. *Sci. Rep.* 14 (1), 535. <https://doi.org/10.1038/s41598-023-49849-w>.
- Stauber, H., Waisman, D., Korin, N., Sznitman, J., 2017. Red blood cell dynamics in biomimetic microfluidic networks of pulmonary alveolar capillaries. *Biomicrofluidics* 11 (1), 014103. <https://doi.org/10.1063/1.4973930>.
- Suckling, K., 2014. Atherosclerosis. In: *Reference Module in Biomedical Sciences*, vol. 1. Elsevier, pp. 1–8. <https://doi.org/10.1016/B978-0-12-801238-3.00190-2>. Issue c.
- Turner, S., Voogt, J., Davidson, M., Glass, A., Killion, S., Decaris, J., Mohammed, H., Minehira, K., Boban, D., Murphy, E., Luchoomun, J., Awada, M., Neese, R., Hellerstein, M., 2012. Measurement of reverse cholesterol transport pathways in humans: in vivo rates of free cholesterol efflux, esterification, and excretion. *J. Am. Heart Assoc.* 1 (4). <https://doi.org/10.1161/JAHA.112.001826>.
- Tziakas, D.N., Chalikias, G.K., Stakos, D., Tentis, I.K., Thomaidi, A., Chatzikyriakou, S., Mitrousi, K., Kortsaris, A.X., Carlos Kaski, J., Boudoulas, H., Konstantinides, S., 2009. Statin use is associated with a significant reduction in cholesterol content of erythrocyte membranes. A novel pleiotropic effect? *Cardiovasc. Drugs Ther.* 23 (6), 471–480. <https://doi.org/10.1007/s10557-009-6202-7>.

- Undas, A., Brummel-Ziedins, K.E., Mann, K.G., 2005. Statins and blood coagulation. *Arterioscler. Thromb. Vasc. Biol.* 25 (2), 287–294. <https://doi.org/10.1161/01.ATV.0000151647.14923.ec>.
- Valverde, M.G., Mille, L.S., Figler, K.P., Cervantes, E., Li, V.Y., Bonventre, J.V., Masereeuw, R., Zhang, Y.S., 2022. Biomimetic models of the glomerulus. *Nat. Rev. Nephrol.* 18 (4), 241–257. <https://doi.org/10.1038/s41581-021-00528-x>.
- van Batenburg-Sherwood, J., Balabani, S., 2022. Continuum microhaemodynamics modelling using inverse rheology. *Biomech. Model. Mechanobiol.* 21 (1), 335–361. <https://doi.org/10.1007/s10237-021-01537-2>.
- Vayá, A., Martínez Triguero, M., Réganon, E., Vila, V., Martínez Sales, V., Solá, E., Hernández Mijares, A., 2008. Erythrocyte membrane composition in patients with primary hypercholesterolemia. *Clin. Hemorheol. Microcirc.* 40 (4), 289–294. <https://doi.org/10.3233/CH-2008-1139>.
- Vogt, L., Bangalore, S., Fayyad, R., Melamed, S., Hovingh, G.K., DeMicco, D.A., Waters, D.D., 2019. Atorvastatin has a dose-dependent beneficial effect on kidney function and associated cardiovascular outcomes: post hoc analysis of 6 double-blind randomized controlled trials. *J. Am. Heart Assoc.* 8 (9). <https://doi.org/10.1161/JAHA.118.010827>.
- Zhou, Q., Fidalgo, J., Calvi, L., Bernabeu, M.O., Hoskins, P.R., Oliveira, M.S.N., Krüger, T., 2020. Spatiotemporal dynamics of dilute red blood cell suspensions in low-inertia microchannel flow. *Biophys. J.* 118 (10), 2561–2573. <https://doi.org/10.1016/j.bpj.2020.03.019>.
- Zhou, Q., Schirrmann, K., Doman, E., Chen, Q., Singh, N., Selvaganapathy, P.R., Bernabeu, M.O., Jensen, O.E., Juel, A., Chernyavsky, I.L., Krüger, T., 2022. Red blood cell dynamics in extravascular biological tissues modelled as canonical disordered porous media. *Interface Focus* 12 (6). <https://doi.org/10.1098/rsfs.2022.0037>.